Microsc. Microanal. 18, 568–581, 2012
doi:10.1017/S1431927612000384

Microscopy AND Microanalysis

Microstructural and Chemical Characterization of Nanostructured TiAlSiN Coatings with Nanoscale Resolution

Vanda Godinho,[1,2,*] Teresa C. Rojas,[1] Susana Trasobares,[3] Francisco J. Ferrer,[4] Marie-Paule Delplancke-Ogletree,[2] and Asuncion Fernández[1]

[1]*Instituto de Ciencia de Materiales de Sevilla CSIC-Uni. Sevilla, Avenida Américo Vespucio 49, 41092 Sevilla, Spain*
[2]*Université Libre de Bruxelles, Chemicals and Materials Department, Faculty of Applied Sciences, Avenue F.D. Roosevelt, 50 (CP165/163), 1050 Bruxelles, Belgium*
[3]*Departamento de Ciencia de los Materiales e Ingeniería Metalúrgica y Química Inorgánica, Facultad de Ciencias, Universidad de Cádiz, Puerto Real, 11510-Cádiz, Spain*
[4]*Centro Nacional de Aceleradores, Parque Tecnológico Cartuja 93, 41092 Sevilla, Spain*

Abstract: Nanoscale resolution electron microscopy analysis combined with ion beam assisted techniques are presented here, to give answers to full characterization of morphology, growth mode, phase formation, and compositional distribution in nanocomposite TiAlSiN coatings deposited under different energetic conditions. Samples were prepared by magnetron sputtering, and the effects of substrate temperature and bias were investigated. The nanocomposite microstructure was demonstrated by the formation of a face-centered cubic (Ti,Al)N phase, obtained by substitution of Al in the cubic titanium nitride (c-TiN) phase, and an amorphous matrix at the column boundary regions mainly composed of Si, N (and O for the samples with higher oxygen contents). Oxygen impurities, predicted as the principal responsible for the degradation of properties, were identified, particularly in nonbiased samples and confirmed to occupy preferentially nitrogen positions at the column boundaries, being mainly associated to silicon forming oxynitride phases. It has been found that the columnar growth mode is not the most adequate to improve mechanical properties. Only the combination of moderate bias and additional substrate heating was able to reduce the oxygen content and eliminate the columnar microstructure leading to the nanocomposite structure with higher hardness (>30 GPa).

Key words: scanning transmission electron microscopy, energy loss spectroscopy, high-angle annular dark field, TiASiN thin films

Introduction

Microstructural design gives the possibility of tailoring the properties of composite materials. The formation of nanocomposites combining nanocrystalline (nc-) hard phases in an amorphous matrix (a-) allows production of materials with improved mechanical properties.

Ternary and quaternary systems of metal nitrides are of great interest, in particular when applied to nanostructured coatings of the Ti-Al-Si-N system with high hardness and good resistance to high-temperature oxidation (Carvalho et al., 2001; PalDey & Deevi, 2003; Veprek & Jilek, 2003; Barshilia et al., 2010). The base concept for the design of superhard nc-TiAlN/a-Si_3N_4 is based on a complete, thermodynamically driven and diffusion rate controlled (spinodal) phase segregation that leads to the formation of a stable nanostructure by self-organization (Veprek & Reiprich, 1995). The envisaged microstructure for hard TiAlSiN coatings consists of a nanocomposite structure formed by TiN-based nanocrystals of 3–5 nm separated by a SiN-based amorphous phase (Veprek & Reiprich, 1995; Park & Kim, 2003; Veprek et al., 2005*b*; Mayrhofer et al., 2006; Zhang & Veprek, 2006), corresponding to typical compositional ranges of 5–12 at.% Si and 10–15 at.% Al (Hauert & Patscheider, 2000; Carvalho et al., 2001) for optimized coatings.

Although nanocomposite coatings of the TiAlSiN system have been widely explored due to their outstanding mechanical properties, some aspects concerning their microstructure and impurities incorporation, as well as their influence on the performance of these coatings, are still under discussion (Carvalho et al., 2009; Veprek et al., 2010). To the best of our knowledge, no previous studies have been reported on the application of advanced high-resolution analytical electron microscopy and specific ion beam techniques to the investigation of these coatings.

It is still not completely elucidated whether or not solid solutions are formed at the TiN-based nanocrystalline phase by substitution of Ti by Al or Si. The similar lattice parameters found for small incorporations of Al or Si in the TiN lattice (Soderberg et al., 2006; Godinho et al., 2010*b*) make it very difficult to identify the phases formed by X-ray diffraction or by transmission electron microscopy with selected area electron diffraction (TEM/SAED). Under adequate experimental conditions fully segregated TiAlN and Si_3N_4 phases can be achieved through spinodal decomposition by formation of crystalline TiN-based grains, embedded in an amorphous SiN-based matrix (Christiansen et al., 1998; Veprek et al., 2005*b*; Mayrhofer et al., 2006; Zhang &

Received July 12, 2011; accepted February 24, 2012
*Corresponding author. E-mail: godinho@icmse.csic.es

Table 1. Deposition Conditions.

Deposition Parameters	Adhesion Layer	Coating	
Working pressure (Pa)	6.67 Ar	1.33 N_2	
Target composition	Ti_3Al	Ti_3Al	Si
and Magnetron power supply	(99.8% purity)	(99.8% purity)	(99.999% purity)
	250 W	600 W	250 W
Substrate bias	−100V	0, −300 V	
Additional substrate heating	—	—, 300°C	
Deposition time	1 h	2.5 h	

Veprek, 2006). According to the work of Zhang and Veprek (2006), enough nitrogen pressure seams to control the phase separation avoiding the appearance of silicide phases. The 6 at.% Si has been reported to produce the smallest grain size for the crystalline TiN-based phase and the highest hardness (Veprek & Reiprich, 1995; Park & Kim, 2003; Veprek et al., 2005*b*; Mayrhofer et al., 2006; Zhang & Veprek, 2006). However, in low energetic conditions the phase separation is not completely achieved and the formation of solid solutions with a face-centered cubic (fcc) structure, where Si atoms substitute some of the Ti positions, has been proposed (Vaz et al., 1999, 2000). The study of Al or Si incorporation in the TiN lattice is therefore an objective of study in this article.

The main reason for the deterioration of mechanical properties is pointed out to be the presence of impurities, mainly oxygen desorbed from chamber walls or from the residual vacuum (Veprek et al., 2005*a*; Hao et al., 2006*c*). The high reactivity of Ti, Al, and Si toward oxygen makes it very difficult to avoid its contamination. Oxygen impurities are foreseen to diffuse to the interface region between nanocrystals and occupy nitrogen sites causing a severe reduction of the mechanical properties (Hao et al., 2006*c*). The role of oxygen on the tensile strength of nc-TiN/a-Si_3N_4 coatings was theoretically investigated by Hao and co-workers (2006*c*). The incorporation of oxygen at the SiN-based interface caused a notable reduction in the tensile strength of the interface in coatings deposited under N-rich conditions, leading to a decrease of hardness. Even 1.54 at.% oxygen is enough to produce an important decrease in the mechanical properties. Veprek et al. (2010) refer to how oxygen can hinder the phase segregation in TiSiN system and stabilize amorphous structures. The evaluation and location of oxygen contamination in nanocomposite films are therefore of extreme importance and will be investigated in the present article to determine the way that mechanical properties are affected and compared to theoretical studies (Veprek et al., 2005*a*; Hao et al., 2006*a*, 2006*b*).

Finally, in this work the influence of deposition parameters, such as substrate bias and temperature, will be related not only to phase formation and oxygen contamination but also to the morphology and growth mode of the coatings that also affects the mechanical properties strongly.

Due to the nanocomposite character of these coatings, the application of energy filtering and high-angle annular dark-field (HAADF) imaging, combined with electron energy loss spectroscopy (EELS), electron diffraction, Rutherford backscattering (RBS), and particle-induced X-ray emission (PIXE), will strongly contribute to elucidate the above-described open questions in this quaternary TiAlSiN nanocomposite system. The study is also relevant because similar questions regarding microstructure, interface composition analysis, and element diffusion in nanocomposite coatings are of prime interest nowadays and our results show the potentiality of advanced microscopy and microanalysis methodologies in this field.

Materials and Methods

Samples Deposition

To study the influence of deposition parameters such as substrate bias and temperature on the microstructure and impurities incorporation on TiAlSiN coatings, four samples deposited under different conditions of substrate temperature and bias, presenting different mechanical properties, were selected. These samples were deposited by reactive magnetron sputtering from a Ti-Al alloy target (75/25 at.%, 99.8% purity, GfE Metalle und Materiallen GmbH, Nuremberg, Germany) and a pure Si target (99.999% purity, Kurt J. Lesker Company, Clairton, PA, USA). Table 1 summarizes the deposition conditions, and details of the deposition system have been described elsewhere (Philippon et al., 2011). Table 2 describes the selected samples and the thickness measured by cross-section scanning electron microscopy (SEM). The diameter of the sputtering guns was 2 in. The samples were deposited on Si wafer (100) substrates. For PIXE analysis, samples deposited simultaneously on mirror polished AISI M2 were also used. The substrates were first degreased using acetone and finally dried with nitrogen. After loading, the vacuum chamber was evacuated to a base pressure of 1.5×10^{-3} Pa. The targets and substrates were sputter cleaned before deposition in an argon atmosphere. For better adhesion between the coating and the substrate, an adhesion layer of TiAl with a thickness of approximately 200 nm was deposited prior to the coating. For the TiAl interlayer deposition, the argon pressure was of 6.67 Pa and the bias voltage was maintained at −100 V. According to the work of Zhang and Veprek (2006), the TiAlSiN coatings were deposited in a pure N_2 atmosphere of 1.33 Pa to favor the spinodal phase decomposition. To study the influence of substrate bias on the microstructure of the coatings, the substrates were nega-

Table 2. Sample Identification.

Sample	Target Ti_3Al (W)	Target Si (W)	Substrate Temperature (°C)	Substrate Bias (W)	Gas Mixture	Thickness (nm)
TiAlSIN(O)/600-250	600	250	—	—	100%N_2	2,096
TiAlSIN(O)/600-250/b	600	250	—	25	100%N_2	1,960
TiAlSIN(O)/600-250/h	600	250	300	—	100%N_2	2,000
TiAlSIN(O)/600-250/hb	600	250	300	25	100%N_2	1,700

tively biased to 25 W radiofrequency (rf) (corresponding to a dc bias of −300 V, value supplied by the rf source). In some coatings the substrate temperature was kept at 300°C by resistive heating. Also coatings without additional substrate heating were deposited (deposition temperature around 200°C). Working in conditions where no substrate bias or additional heat is employed makes it possible to have samples with high enough oxygen content to investigate its incorporation in the coatings.

The label of the samples indicates first, the power (in W) supplied to the Ti_3Al target; second, the power supplied to the Si target; and third, the applied additional temperature (h) and/or substrate bias (b).

Samples Characterization

The morphology and thickness of the coatings were investigated by SEM performed in a high-resolution field emission gun (FEG) microscope, Hitachi S4800 (Hitachi, Kanagawa, Japan). Samples grown on silicon substrates were used for the SEM analysis. Cross-section samples were obtained by cleavage of the silicon pieces.

For the TEM studies two microscopes operating at 200 kV have been used:

1. a Philips CM200 equipped with a parallel detection electron energy loss spectrometer from Gatan (766-2 kV) (Gatan, Inc., Pleasanton, CA, USA)
2. a JEOL JEM 2010F (JEOL Ltd., Tokyo, Japan), scanning electron transmission FEG microscope, equipped with a HAADF detector and an imaging filter from Gatan GIF2000. For the spectrum imaging mode, a 0.5 nm beam with a current of 0.1–0.3 nA scanned along the sample area was used. The HAADF signal was also simultaneously collected at each point within the scanned area.

The Gatan Digital Micrograph software was used to measure lattice spacing and to calculate digital diffractograms (fast Fourier transform). The program EjeZ from the University of Cadiz (Perez-Omil, 1994) was used to simulate the digital diffraction pattern (DDP).

TEM cross-sectional samples were prepared by the focused ion beam technique using a FEI Quanta three-dimensional environmental scanning electron microscope (FEI Company, Hillsboro, OR, USA). The samples were thinned to approximately 100 nm using Ga ions with an acceleration voltage of 30 kV and a current of 10 pA at the ion source. Also planar view samples were prepared by mechanical polishing followed by Ar+ ion milling to electron transparence using a Baltec RES 100 system (Baltec Corporation, Canonsburg, PA, USA). The final thinning was done using a low energy condition (low angle 6°, voltage 3 kV, and a current of 3 mA) to remove the damage.

Ion beam analysis techniques were performed using the 3 MV tandem accelerator of the National Centre for Accelerators (Seville, Spain). RBS was carried out with a surface barrier detector set at 165° and He ions at 3,045 keV so that a resonance for oxygen was possible. PIXE was carried out with a Si(Li) detector placed at 135° using a 3.4 MeV He beam. Samples grown on Si were used for RBS measurements and samples deposited on AISI M2 steel (deposited simultaneously) were used for PIXE measurements to avoid the big Si signal from the substrate.

Additional measurements, not shown in this work, demonstrate that no change in thickness and composition (as measured by X-ray photoelectron spectroscopy) was found for coatings grown onto the two selected substrates: silicon and AISI M2 steel.

Results and Discussion

Compositional Analysis, Morphology, Texture, and Electron Diffraction

One of the major problems in the characterization of impurities in coatings composed by elements with high affinity to oxygen is its oxidation when exposed to air. Surface analysis techniques are therefore not appropriate. The use of ion beam techniques allows acquisition of the chemical composition of the bulk sample avoiding overestimation of surface oxygen contamination. The combined use of RBS and PIXE deserves special mention here as a useful tool to determine composition in this type of coating. Many authors use RBS to evaluate the chemical composition of their coatings commonly at ∼2 MeV He^+ (Carvalho et al., 2001; Ribeiro et al., 2002; Nakonechna et al., 2004); however, in such conditions it is not possible to distinguish the O signal from the one of Al + Si. In addition, at ∼2 MeV He^+ the whole depth of the sample cannot be analyzed. Simulated RBS spectra for both 1,800 and 3,045 keV He^+ ion beams can be found in Figure 1a for a sample composed of a coating of 2,100 nm thickness containing 26% Ti, 11% Al, 6% Si, 48% N, and 9% O (at.%) and an underlayer of 200 nm containing 75% Ti and 25% Al (at.%). Simulation

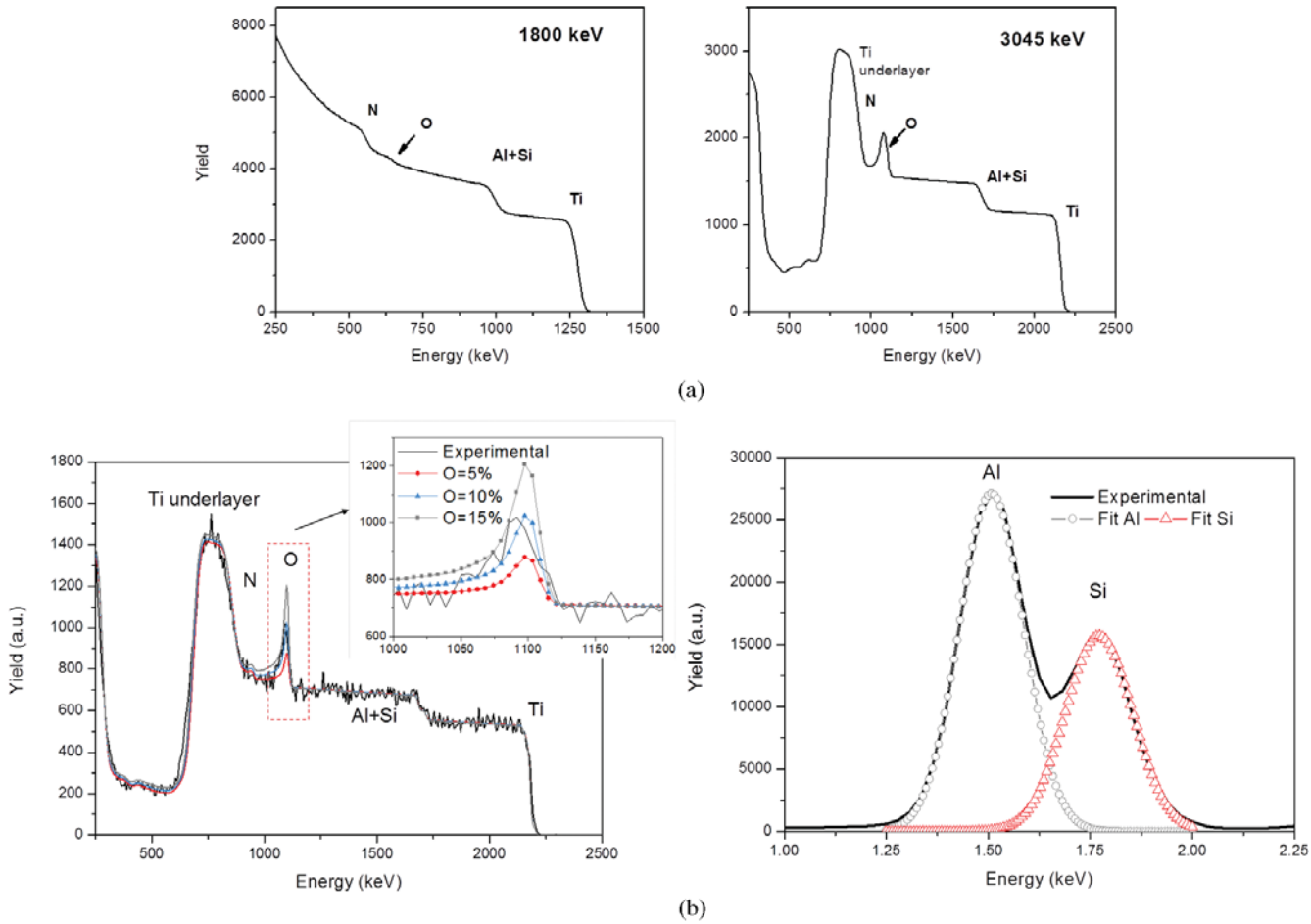

Figure 1. **a:** Simulated RBS spectra of a representative TiAlSiN(O) sample measured at 1,800 keV and 3,045 keV. **b:** Left: Experimental and simulated RBS profile of sample TiAlSiN(O)/650-250; the inset shows the zone where O resonance is detected; right: peaks at Al and Si emission of PIXE spectra for the same sample.

and analysis of spectra were done using the SIMNRA simulation code (Mayer, 1997). The energy of 3,045 keV was therefore selected to improve oxygen signal giving a method for oxygen analysis in this type of coating with an error of ca. 10%.

In addition the mass resolution in the RBS spectra was not good enough to separate the signals from Al and Si. This drawback was solved by fitting the RBS (sample on Si substrate) and PIXE (sample on steel substrate) spectra assuming the same atomic composition for samples deposited simultaneously on Si and steel substrates. In fact, the Si/Al ratio can be readily determined by PIXE (see spectrum in Fig. 1b), and these data were used in the RBS spectra to find the Al contribution from the TiAlSiN nanostructured coating and the one from the TiAl adhesion layer. Combining these two methods, the relative proportion of the heavier elements (Si, Al, and Ti) was determined with an error of ca. 7%.

Bulk composition of the selected coatings given by ion beam analysis techniques (RBS + PIXE) is summarized in Table 3. The coatings present similar composition and are composed mainly by Ti, Al, Si, and N presenting a Ti/Al ratio around 3, corresponding to the composition of the Ti_3Al target. As expected, small amounts of O impurities (maximum 9 at.%) are found in the case of the samples deposited without substrate bias and additional heating, while in the samples deposited with substrate bias, the oxygen signal was below the detection limits of these techniques (below 5 at.% the signal starts to be difficult to quantify, see Fig. 1b). Bias seems to therefore contribute to avoidance of oxygen contamination of the films.

The data in Table 3 also show a decrease in nitrogen content when oxygen impurities are detected, keeping approximately the same amount of Ti, Al, and Si for all samples, which seems to indicate that oxygen when incorporated replaces nitrogen in the coatings. The selected compo-

Table 3. Chemical and Elemental Composition Given by RBS and PIXE.

	Composition (at.%)				
Sample	Ti	Al	Si	N	O
TiAlSiN(O)/600-250	26	11	6	48	9
TiAlSiN(O)/600-250/b	27	7	6	60	—
TiAlSiN(O)/600-250/h	25	11	7	51	6
TiAlSiN(O)/600-250/hb	26	11	8	55	—

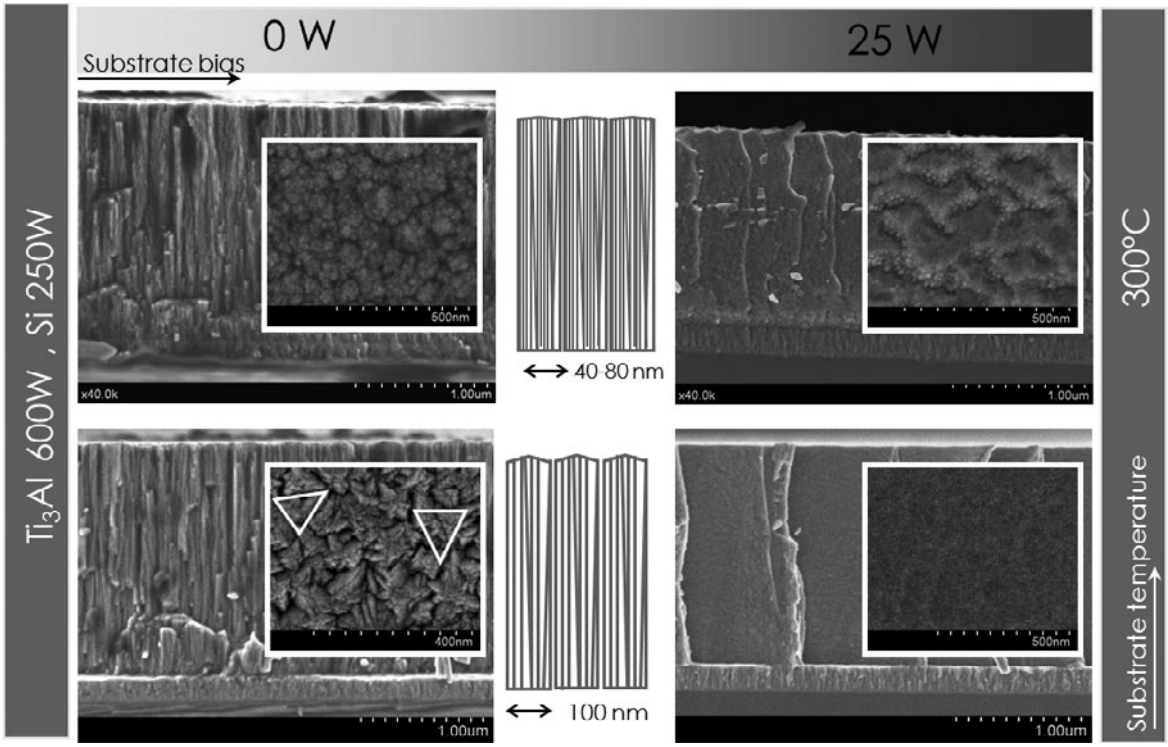

Figure 2. SEM planar view and cross section of the samples with and without bias and with and without additional heating.

sitions are in the range of those for optimized coatings (Veprek & Reiprich, 1995; Park & Kim, 2003; Veprek et al., 2005*b*; Mayrhofer et al., 2006; Zhang & Veprek, 2006) presenting superhardness; however, the amount of O for nonbiased samples is much higher than allowed for hard coatings. However, the deposition conditions have been selected to improve the signal-to-noise ratio for the detection of Si-based phases and O location that is one main objective of this article.

Apart from the oxygen contamination as previously mentioned, the microstructure also plays a decisive role on coatings properties. In this sense, the influence of substrate bias voltage and additional temperature on the morphology, growth mode, and phase formation of the coatings was first analyzed. The effects of both temperature and substrate bias on the growth mode of several thin films have been described by many authors (Thornton, 1977; Mahieu et al., 2006; Anders, 2010). SEM images of the selected samples are presented in Figure 2. From the cross-sectional images, it is possible to distinguish the Ti-Al adhesion layer with a thickness of ~200 nm and the coating. The nonbiased samples show columnar structure typical of coatings deposited under low energetic conditions, corresponding to zone I of Thornton's diagram. Zone 1 of Thornton's model occurs at Ts/Tm (Ts is the substrate temperate and Tm is the material melting point) so low that surface diffusion is negligible; shadowing processes are responsible for the columnar growth, separated by voids of few nanometers (Thornton, 1977). A detailed observation allows identification of a structure of mesocolumns (understanding that meso is between micro and nano) formed by aggregates of smaller columns (nanocolumns) that end in a pyramidal shape for the sample without additional heating as can be clearly seen in the planar view images. When additional heating is applied, the columnar structure is now composed of finer columns with smaller voids separating them, giving a cauliflower look to the coating surface, instead of triangular ending mesocolumns. A schematic representation of these microstructures is presented in Figure 2.

When substrate bias is applied, there is an increase in the adatom mobility, and resputtering effects can occur, which can eliminate the open voids and introduce overlapping of the grains resulting in more dense structures (Tanaka et al., 2001).

Finally when substrate bias and additional substrate temperature are employed (sample TiAlSiN(O)/600-250/hb), the resputtering effects are stronger and responsible for the rough surface and the decrease in thickness as compared to the sample deposited without additional temperature.

The morphology and crystallinity of the coatings were evaluated in more detail by cross-section transmission electron microscopy (XTEM) and SAED. In Figure 3 XTEM micrographs of the samples and the respective SAED are presented.

As expected from the SEM micrographs, the samples deposited without substrate bias (TiAlSiN(O)/600-250 and TiAlSiN(O)/600-250/h) and in particular the one prepared with no additional substrate temperature (TiAlSiN(O)/600-250) have a pronounced columnar structure (see Fig. 2) where it is possible to identify the mesocolumns (40–

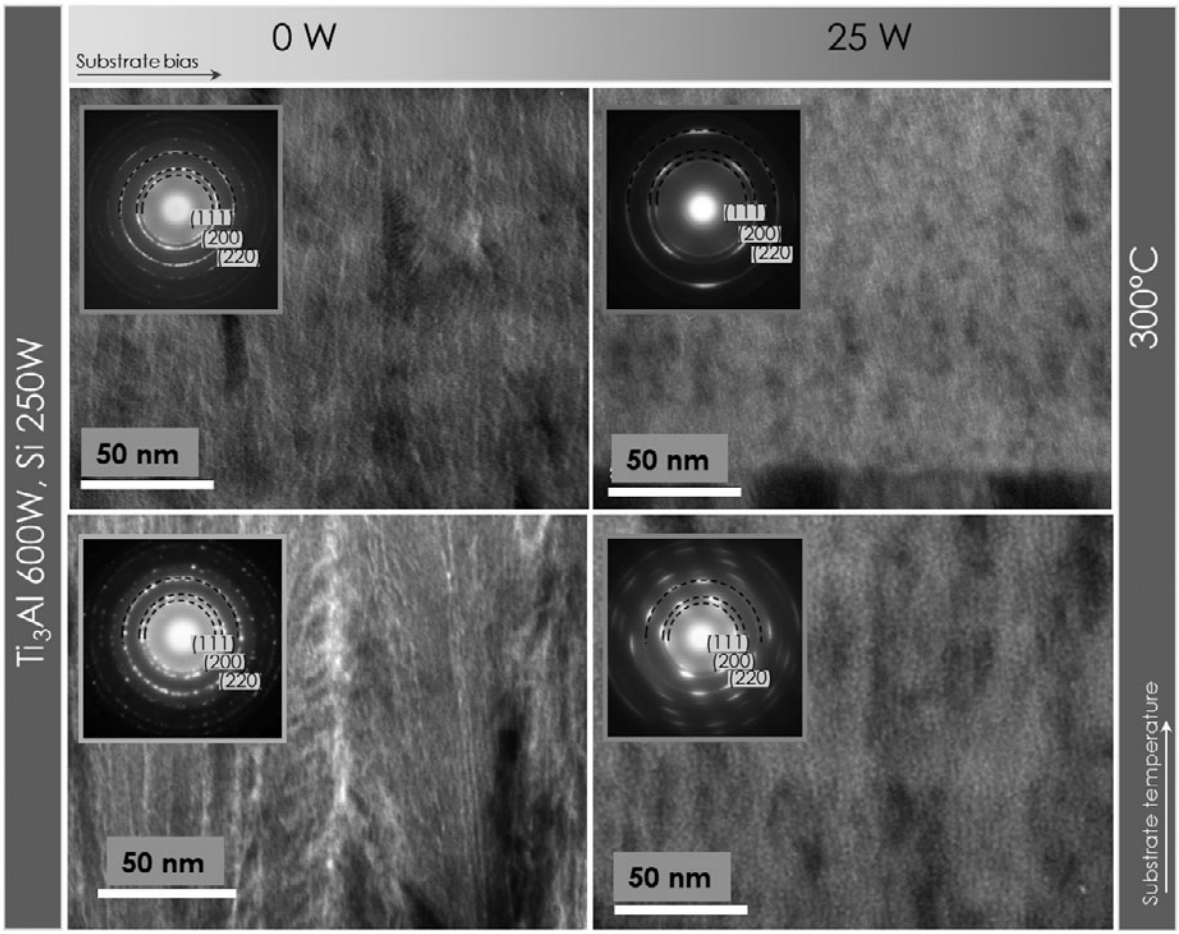

Figure 3. TEM cross-sectional views of the coatings and respective SAED pattern.

100 nm), which are composed by nanocolumns (of 5–20 nm). The column boundaries and voids can be identified by the bright contrast between them. The width of the boundaries between the mesocolumns is bigger than between the nanocolumns for the sample prepared without additional substrate temperature. As already observed by SEM, the biased samples appear to be denser and will be analyzed below in more detail.

The SAED pattern, included in the insets of Figure 3, present diffraction rings indicating the formation of polycrystalline phases. Moreover, from the SAED pattern it is possible to say that the nonbiased samples present a random orientation of the nanocrystals, whereas in the samples prepared with substrate bias, there is preferred orientation for the nanocrystals. The indexation of the rings recorded from the coating can be assigned to the family of planes {111}, {200}, and {220} corresponding to cubic TiN-based phases. From these data it is not possible to determine if Al or Si are substituting Ti in the TiN lattice to form solid solutions.

Figure 4 shows in the left-hand side that the apparently dense structure shown by SEM for biased samples is in fact formed by columns in the growing direction for the sample grown without additional heating. The column boundaries are difficult to appreciate, but from differences in contrast one can say that the coating also has a structure formed by narrow nanocolumns (around 6 nm wide) as can be observed in more detail in the right-hand side of Figure 4. When substrate bias and additional temperature are present, the structure becomes more compact and the columnar structure completely disappears as expected from SEM micrographs. In the high-resolution TEM (HRTEM) image in Figure 4 (right side), the measured d spacing of the lattice fringes are 2.4 Å and 2.1 Å, which can also be assigned to the 111 and 200 planes, respectively, of cubic TiN-based phases. As can be observed the size of the crystals along the growing direction is smaller than the thickness of the coating, indicating that the nanocolunms are polycrystalline formed by several nanocrystals of TiAlN.

In Figure 5a a high-resolution planar view TEM image of sample TiAlSiN(O)/600-250/b shows small 2 to 10 nm crystals embedded in an amorphous matrix with a width of 0.5–1.2 nm. The insets in this figure correspond to the DDP obtained from the two marked areas. The values of 2.1, 2.4, and 1.5 Å measured in the marked area of Figure 5 can be assigned to 200, 111, and 202 planes of the cubic face centered TiN-based phase and the geometry of the sets of spots in the two insets corresponds to the [011] and [111] zone axis of this phase. It is important to emphasize here that the geometric arrangement and intensities of the simu-

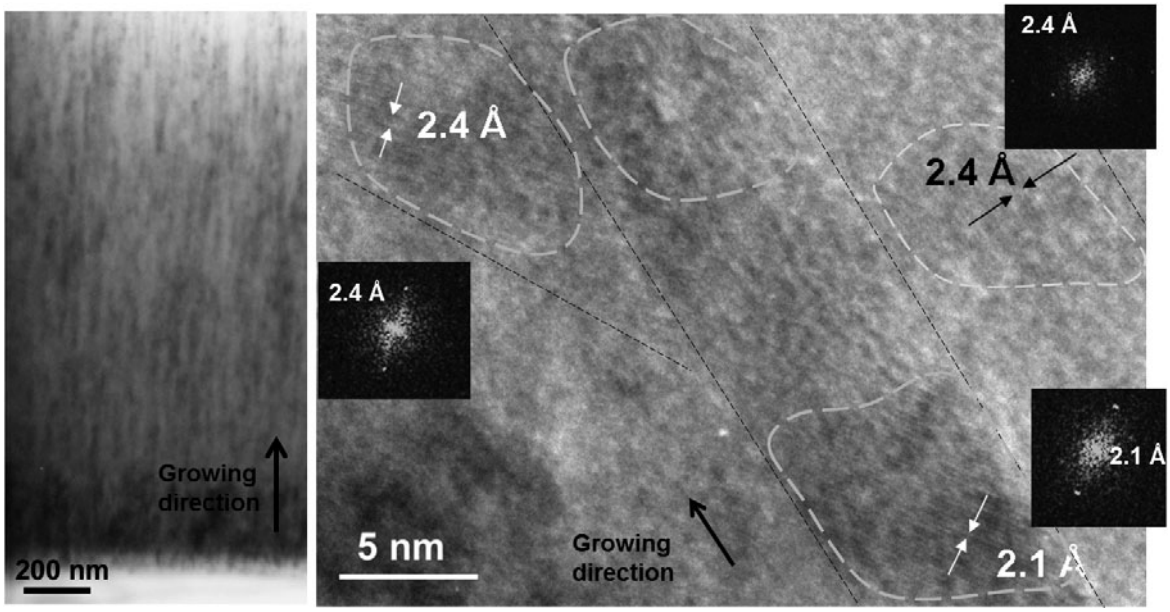

Figure 4. (**a**) High magnification micrograph and (**b**) HRTEM micrograph from the cross section showing three crystal and its interplanar distances of sample TiAlSiN(O)/600-250/b.

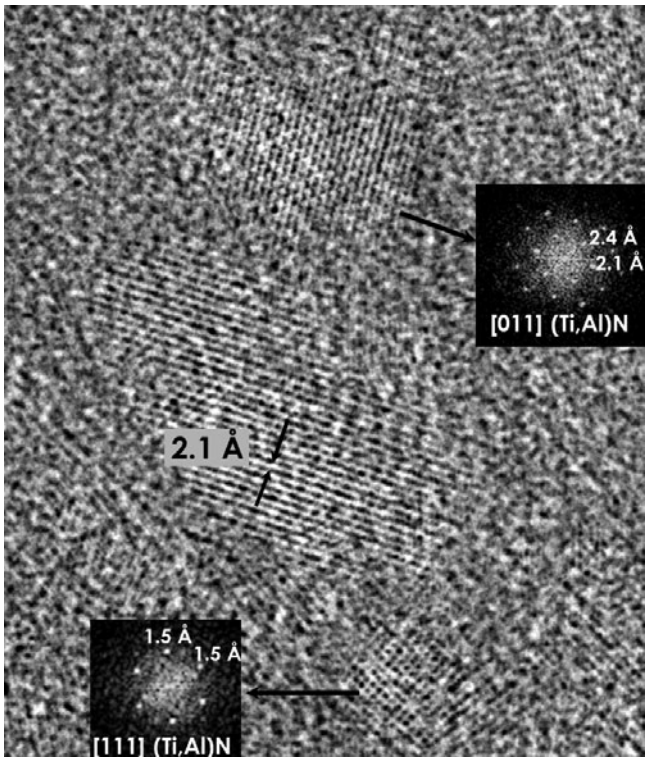

Figure 5. HRTEM planar view of sample TiAlSiN(O)/600-250/b.

lated DDP pattern for a stoichiometric Ti_3AlN phase (from Ti 75%, Al 25% target) were not observed, indicating that the Al atoms, if incorporated, are most probably occupying Ti sites in a nonordered way, and a nonstoichiometric solid solution phase should be formed. The incorporation of Al or Si to the TiN lattice will be investigated by elemental mapping analysis below in this article. At that point c-TiN and c-(Ti,Al)N phases are possible.

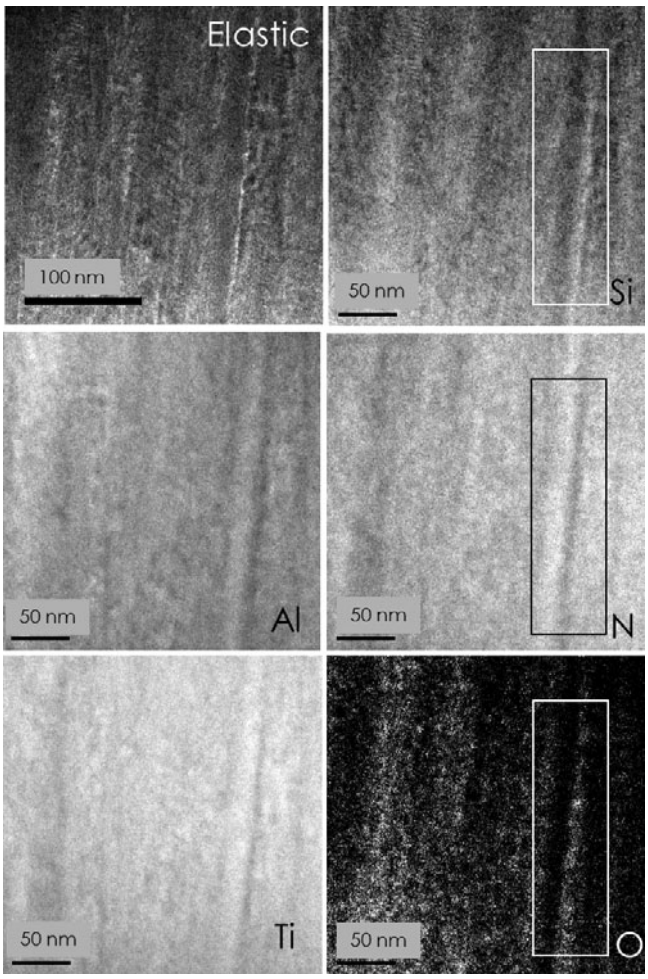

Figure 6. EFTEM micrographs: elastic TEM image and elemental maps for Si, Al, N, Ti, and O. Edges used: Al $L_{2,3}$, Si $L_{2,3}$, N-K, Ti $L_{2,3}$, and O-K.

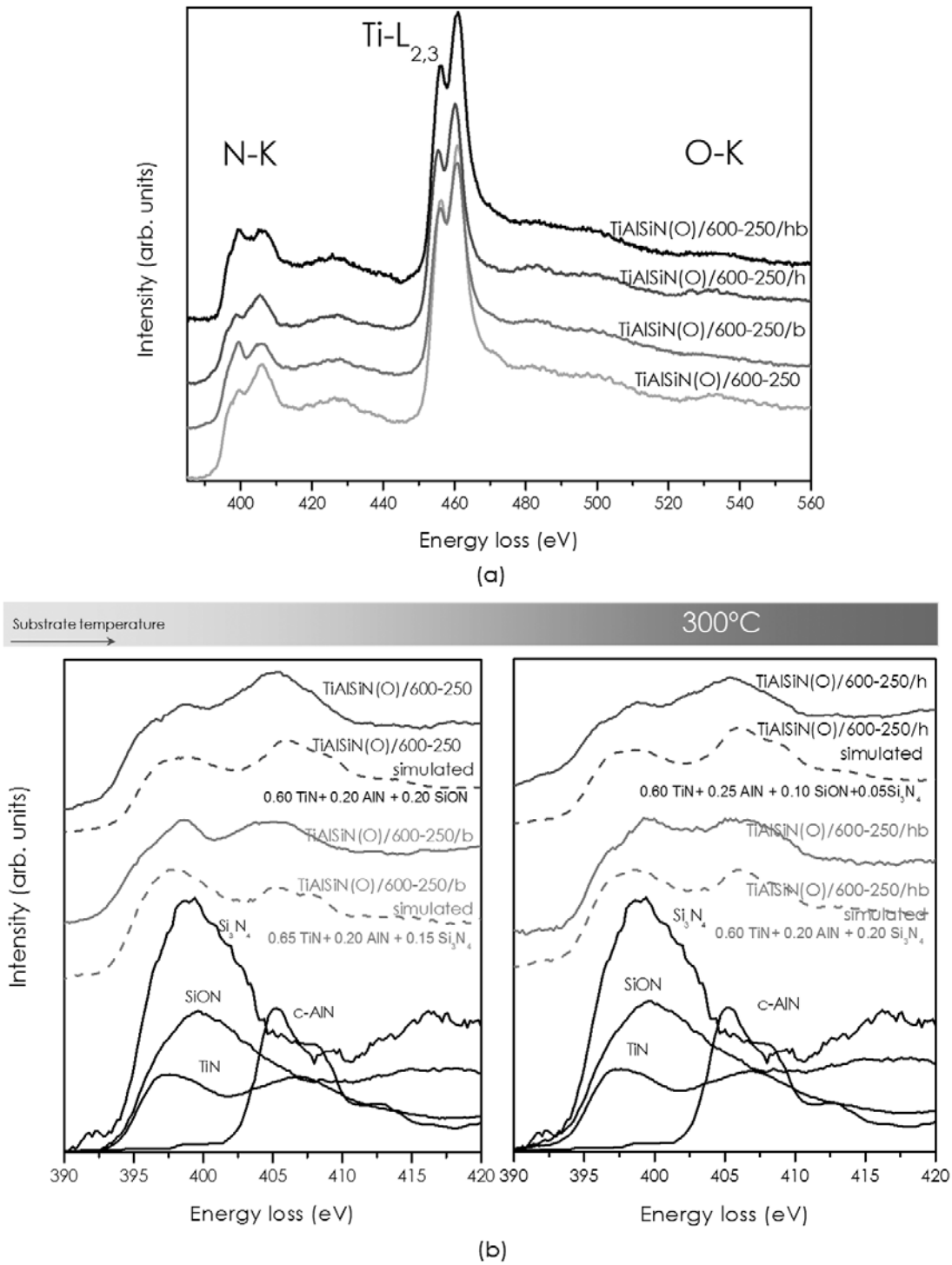

Figure 7. **a:** EELS spectra in the cross section of both samples. **b:** Detail of N-K edge: measured spectra and linear combinations of standard nitrides.

Elemental Maps, EELS, and HAADF Analysis

The Si, Al, Ti, N, and O elemental distribution in the sample prepared without bias and no additional substrate temperature, presenting the higher oxygen content, was studied in more detail by energy-filtering transmission electron microscopy (EFTEM), and a representative area is included in Figure 6. In the elastic image in Figure 6 with high contrast, it is possible to see the columnar growth of the coating and the voids separating the columns. In the elemental maps the white zones correspond to higher intensity of that element. A heterogeneous distribution of the different elements is observed. It is possible to see that the columns are rich in Al, Ti, and N, while the areas richer in Si are also richer in O. These results point out the preferential formation of (Ti,Al)N solid solution crystalline fcc phases (responsible for electron diffraction patterns), while SiON-based phases

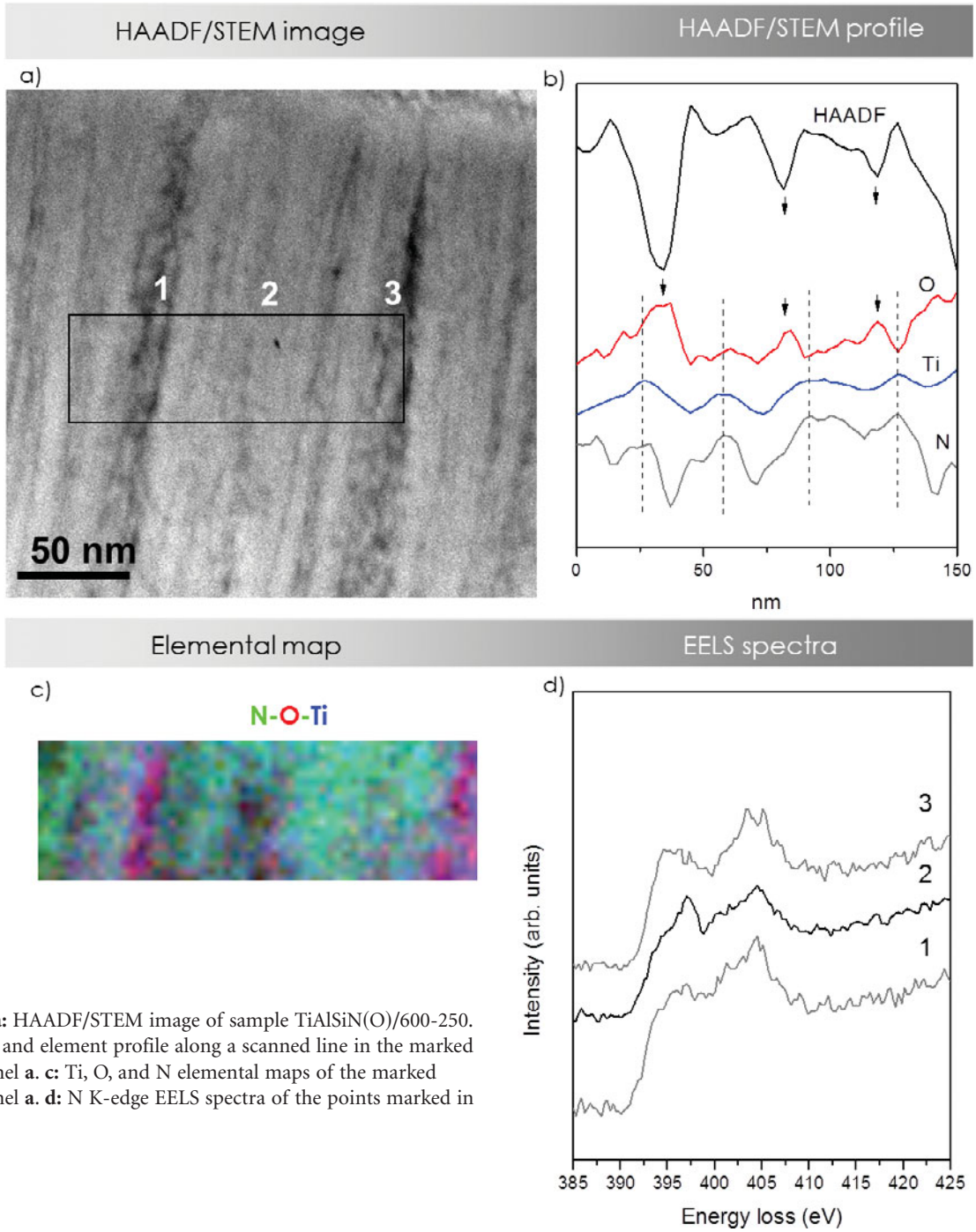

Figure 8. **a:** HAADF/STEM image of sample TiAlSiN(O)/600-250. **b:** HAADF and element profile along a scanned line in the marked zone in panel **a**. **c:** Ti, O, and N elemental maps of the marked zone in panel **a**. **d:** N K-edge EELS spectra of the points marked in panel **a**.

are preferentially forming the amorphous interface matrix. In a closer inspection at the N, Si, and O maps, in the marked interface, an inner core richer in Si and O surrounded by a Si-N-O layer at the amorphous boundary matrix (left side of the marked column) can be proposed.

This result is in agreement with the work of Hao et al. (2006*a*), where the oxygen impurities are predicted to diffuse to the interface region and occupy nitrogen sites. In their work, Hao et al. (2006*a*) considered different scenarios for the evaluation of oxygen incorporation and calculated the preferred oxygen sites. For a nitrogen-rich atmosphere and considering the formation of a Si_xN_y interface, the preferred oxygen sites are substitution sites of nitrogen. This explains a certain deficit of nitrogen in the areas associated to Si. Additional information in this respect will be given below by HAADF/EELS analysis in scanning transmission electron microscopy (STEM) mode with improved lateral resolution. Within our experimental limitations we can conclude that Si-based phases appear separated from TiAl-based phases.

EELS analysis of the cross section of the coatings is a powerful tool in the evaluation of chemical composition allowing determination of the chemical bonding state. It is particularly useful in this case to also determine the incor-

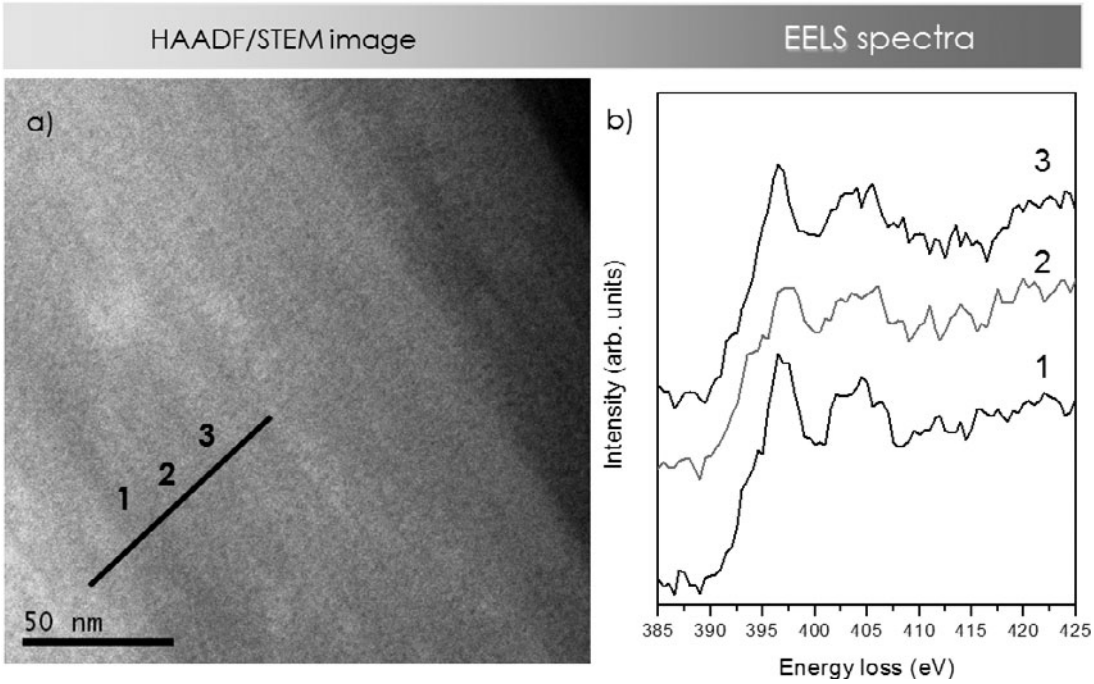

Figure 9. a: HAADF/STEM image of sample TiAlSiN(O)/600-250/b. **b:** N K-edge EELS spectra of the zones marked in panel **a**.

poration of impurities, specifically regarding the oxygen content.

Figure 7a shows the EELS spectra for N-K, Ti-$L_{2,3}$, and O-K edges in the cross section of the coatings from areas of tens of nanometers in diameter. A small oxygen signal is measured in the nonbiased samples that disappears when substrate bias is applied. These results are in good agreement with RBS and PIXE analysis. The changes in the O-K edge are also associated with differences in the N-K edge. Figure 7b presents in detail the N-K edge of the samples. The biased sample presents an increase of intensity of the first peak (located between 393 and 401 eV) of the N-K edge doublet. The N K-edge represents a combination of the contribution of all N containing phases according to their present amount.

The main difference in composition between these coatings is the O content. As previously described it is expected that impurities go to the amorphous boundary phase outside the crystalline c-TiN based phase. In fact a reference coating was prepared using the silicon target in pure N_2 plasma. In these conditions an amorphous SiO_xN_y coating was obtained and characterized (Godinho et al., 2010*a*). It is included in Figure 7b as a reference. According to the nanocomposite structure, the N K-edge should contain the contribution of c-TiN, c-AlN [the c-(Ti,Al)N is also a combination of these two phases (MacKenzie et al., 2005)], SiON, and/or Si_3N_4 phases, following the elemental composition in Table 3. Reference spectra have been included for all these phases normalized to the edge jump at 445 eV. The dashed curves in Figure 7b represent linear combinations of the reference spectra according to each sample composition. The higher intensity of the first peak in the samples is characteristic of the presence of SiON and/or Si_3N_4. The presence of c-AlN [pure or as solid solution c-(Ti,Al)N] also gives a characteristic peak at 402–410 eV.

The spectra of samples deposited with substrate bias are adjusted with the Si_3N_4 phase while nonbiased samples are better adjusted with the spectrum of a SiON phase or a mixture of both as in the case of sample TiAlSiN(O)/600-250/h deposited without substrate bias at 300°C according to measured stoichiometries. This also indicates that when oxygen is present it is preferentially bonded to silicon.

To have chemical information with improved lateral resolution (around 0.5 nm), the spectrum image mode has also been used to obtain EELS spectra from selected areas. Also HAADF/STEM images, obtained at the same area, allowed acquisition of structural and chemical information with the same lateral resolution.

Figure 8 corresponds to the results of the sample deposited under the softer energetic conditions (no additional heating and no bias). Clearly the zones in Figure 8a identified with points 1 and 3 correspond to the area between mesocolumns and point 2 to a mesocolumn. The HAADF signal, nitrogen, titanium, and oxygen profiles obtained across the meso- and nanocolumns (marked zone) are depicted in Figure 8b. A more detailed inspection of the N (gray), Ti (blue), and O (red) signals leads to a correlation between Ti and N; when the titanium signal increases, there is an increase in the nitrogen signal. However, the oxygen signal has its maxima shifted from the maxima of Ti and N and correlates directly with the HAADF signal. This result points again to a depletion of nitrogen when oxygen is incorporated at the boundaries of TiN-based columns. The

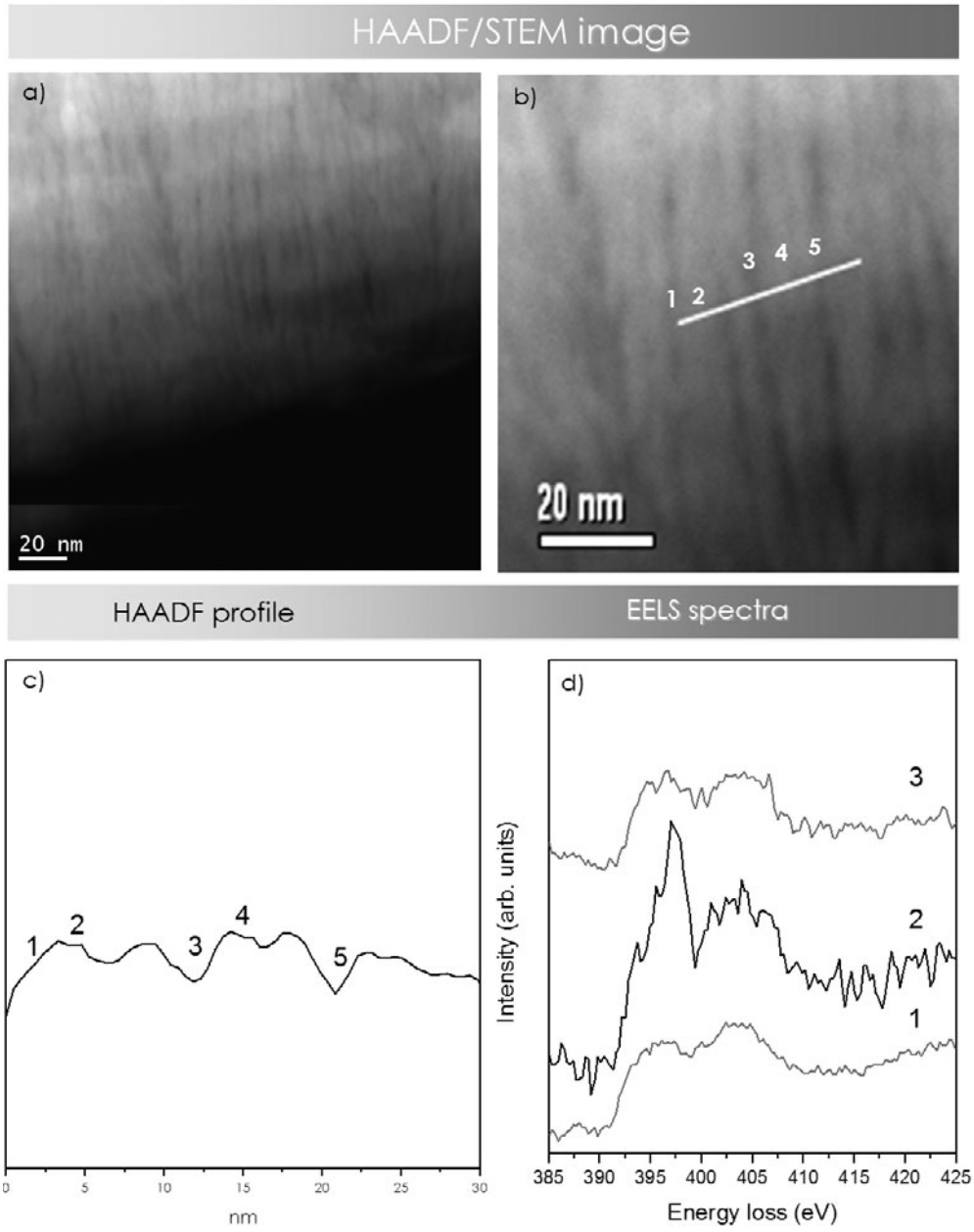

Figure 10. (**a,b**) HAADF/STEM image of sample TiAlSiN(O)/600-250/h; (**c**) HAADF profile and (**d**) N K-edge core level EELS spectra along the scanned line.

N, Ti, and O elemental map in RBG, corresponding to the selected area, is also included in Figure 8c. Oxygen is clearly distributed in the intercolumnar areas.

In Figure 8d the EELS spectra at the N K-edge from the marked points of Figure 8a are presented. The increase of the intensity of the first resonance peak at ca. 397 eV at the mesocolumn region (point 2) corresponds to a smaller contribution of SiON (and a higher contribution of Si_3N_4) in comparison to the area between mesocolumns (points 1 and 3) as already shown in Figure 7.

For the biased sample deposited without additional substrate temperature, Figure 9a shows the HAADF/STEM image showing the columnar structure that is still present under these conditions. The increase in the first peak of the N-K edge (Fig. 9b) corresponds to the formation of (Ti,Al)N and SiN phases. In the nanocolumn area zone 2, this edge is similar to a TiAlN cubic phase (MacKenzie et al., 2005), while interface (zone 1 and 3) consists in a mixture of TiAlN and SiN. See the data in Figure 7.

The effect of substrate temperature during deposition was also investigated by HAADF/STEM images and EELS spectra. Figure 10a shows HAADF/STEM images of the sample deposited at 300°C without substrate bias TiAlSiN(O)/600-250/h. The images show very fine columns (4–9 nm) with very small voids between them (the biggest in the image is 2 nm wide). Once more it is possible to observe differences in the nitrogen K-edge (Fig. 10d) when comparing columns and intercolumnar space. The column marked

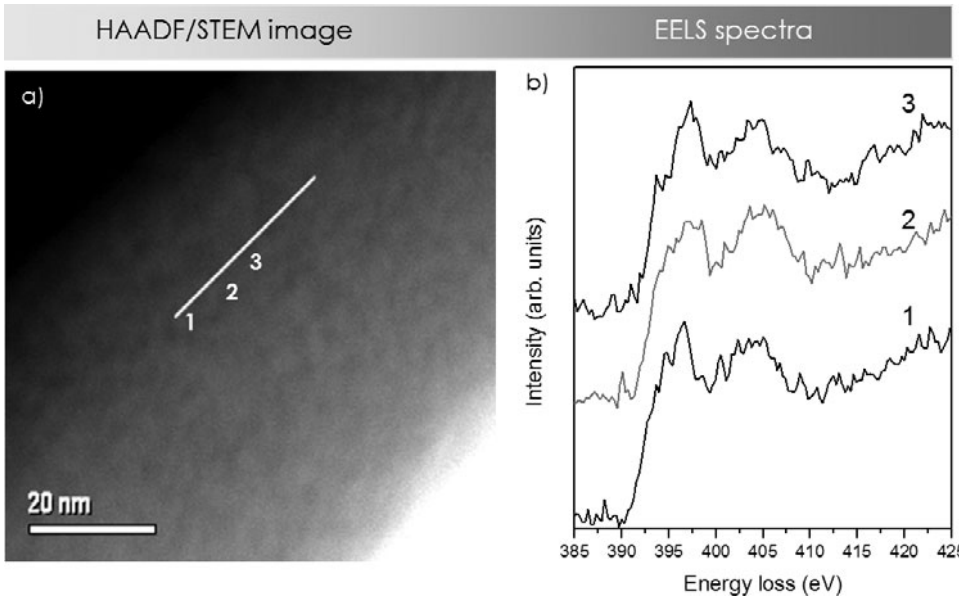

Figure 11. (**a**) HAADF/STEM image of sample TiAlSiN(O)/600-250/hb and (**b**) N K-edge core level EELS spectra along the scanned line.

with 2 present the first peak of the N K-edge doublet higher than the second one, while for the intercolumnar areas marked with 1 and 3, it is lower. The HAADF signal is very useful to monitor columnar and intercolumnar areas as stated in Figure 10c.

The differences in the N K-edge are due not only to the differences in the oxygen content but also to the different phases forming the columns (TiAlN) and the interfaces (SiN) as already discussed for samples grown under bias.

When substrate bias is applied at a substrate temperature of 300°C, the columnar structure completely vanishes and the HAADF profiles are smoother. In Figure 11 the HAADF/STEM image and the N K-edge EELS spectra corresponding to the scanned line are presented. It seems that due to substrate temperature the columnar growth mode disappears and the tridimensional nanocomposite structure makes it more difficult to differentiate the phases due to the fact that the thickness of the sample is high as compared to grain size. The EELS spectra from points with different contrast in the image are more similar indicating this effect.

The measurement of the mechanical properties shows that the coating with the highest oxygen content, prepared under no-bias and no-additional heating (TiAlSiN(O)/600-250), gives low hardness values (<20 GPa). Although biasing is reducing the oxygen content, only the combination of a moderate bias and additional substrate temperature is the condition producing the most important improvement of the mechanical properties leading to coatings of hardness >30 GPa for the TiAlSiN(O)/600-250/hb sample. The location of oxygen at the interface regions between the nanocrystalline and the amorphous phase has been proposed as the main reason to deteriorate the mechanical properties of the coatings (Veprek et al., 2005*a*; Hao et al., 2006*a*). It has been shown in this article that the elimination of the columnar growth mode is also very important by favoring the formation of the nanocomposite structure and favoring the spinoidal phase segregation. Hao et al. (2006*c*) showed how even 1.54 at.% oxygen is enough to produce an important decrease in the mechanical properties. Higher temperatures at the substrate and moderate bias conditions are demonstrated here to be the most effective conditions to reduce oxygen and to improve the segregation of both (Ti,Al)N and SiN phases (Veprek & Reiprich, 1995; Park & Kim, 2003; Veprek et al., 2005*b*; Mayrhofer et al., 2006; Zhang & Veprek, 2006).

Conclusions

Nanostructured coatings of the TiAlSiN system have been prepared and characterized with the support of advanced microscopy and microanalysis tools. The coatings are of prime interest due to their nanocomposite microstructure and good mechanical properties as high hardness and high-temperature resistance.

The quantification and location of the oxygen impurities is a point of high interest in these materials. RBS (coupled to PIXE) has been selected in this article as a powerful tool for determining bulk composition in this type of coating. According to our knowledge we have reported here for the first time the importance of selecting the energy of He^+ ions to achieve a resonance in the oxygen peak as a unique tool to determine oxygen content in these coatings for values around 10 at.% up to 5 at.%.

HRTEM clearly showed the formation of the nanocrystalline and the amorphous phases while the digital diffraction pattern confirmed the formation of the cubic TiN-based crystalline phase also identified by SAED in XTEM. The formation of the c-Ti_3AlN phase has been excluded. The elemental maps obtained by EFTEM confirm the formation of solid solution c-(Ti,Al)N phases. The amorphous matrix at the boundary regions has been identified to be mainly composed of Si, N and O.

The oxygen impurities were identified in particular in nonbiased samples and confirmed to occupy preferentially

nitrogen positions (confirmed by HAADF and EFTEM) at the column boundaries being mainly associated to silicon forming oxynitride phases. A moderate bias has been found very efficient to reduce oxygen impurities in the coatings.

The study of the N-K edge at the interface regions with nanoscale resolution allowed the identification of silicon oxynitride and silicon nitride phases depending on the oxygen content of the samples.

It has been found that the columnar growth mode is not the most adequate to improve mechanical properties. Only the combination of moderate bias and additional heating was able to reduce the oxygen content and to eliminate the columnar microstructure leading to the nanocomposite tridimensional structure with higher hardness. Higher deposition temperatures, cleaner vacuum, and reduced oxygen impurities in targets will be the most adequate conditions to achieve best performance coatings.

This microscopy and microanalysis study reports the strong potential of this methodology to understand the behavior of nanocomposite coatings of this type and coatings in general.

Acknowledgments

The authors are thankful for financial support from the EC (project NoE EXCELL and REGPOT AL-NANOFUNC), Spanish Ministry MICINN (CONSOLIDER FUNCOAT), CSIC (20160I041 and 201060E102), and Junta de Andalucía(TEP 217). The contribution of Dr. Y. Kauffman for the HRTEM image (Electron Microscopy Center at the Faculty of Materials Engineering—Technion, Haifa, Israel) is gratefully acknowledged.

References

Anders, A. (2010). A structure zone diagram including plasma-based deposition and ion etching. *Thin Solid Films* **518**(15), 4087–4090.

Barshilia, H.C., Ghosh, M., Shashidhara, Ramakrishna, R. & Rajam, K.S. (2010). Deposition and characterization of TiAlSiN nanocomposite coatings prepared by reactive pulsed direct current unbalanced magnetron sputtering. *Appl Surf Sci* **256**(21), 6420–6426.

Carvalho, S., Rebouta, L., Cavaleiro, A., Rocha, L.A., Gomes, J. & Alves, E. (2001). Microstructure and mechanical properties of nanocomposite (Ti,Si,Al)N coatings. *Thin Solid Films* **398–399**, 391–396.

Carvalho, S., Rebouta, L., Ribeiro, E., Vaz, F., Tavares, C.J., Alves, E., Barradas, N.P. & Riviere, J.P. (2009). Structural evolution of Ti-Al-Si-N nanocomposite coatings. *Vacuum* **83**(10), 1206–1212.

Christiansen, S., Albrecht, M., Strunk, H.P. & Veprek, S. (1998). Microstructure of novel superhard nanocrystalline amorphous composites as analyzed by high resolution transmission electron microscopy. *J Vac Sci Technol B* **16**(1), 19–22.

Godinho, V., de Haro, M.C.J., Garcia-Lopez, J., Goossens, V., Terryn, H., Delplancke-Ogletree, M.P. & Fernandez, A. (2010*a*). SiOxNy thin films with variable refraction index: Microstructural, chemical and mechanical properties. *Appl Surf Sci* **256**(14), 4548–4553.

Godinho, V., Philippon, D., Rojas, T.C., Novikova, N.N., Yakovlev, V.A., Vinogradov, E.A. & Fernandez, A. (2010*b*). Characterization of Ti1-xAlxN coatings with selective IR reflectivity. *Solar Energy* **84**(8), 1397–1401.

Hao, S., Delley, B. & Stampfl, C. (2006*a*). Role of oxygen in TiN(111)/Si_xN_y/TiN(111) interfaces: Implications for superhard nanocrystalline nc-TiN/a-Si_3N_4 nanocomposites. *Phys Rev B* **74**, 035424.

Hao, S., Delley, B. & Stampfl, C. (2006*b*). Structure and properties of TiN(111)/Si_xN_y/TiN(111) interfaces in superhard nanocomposites: First-principles investigations. *Phys Rev B* **74**(3), 035402.

Hao, S., Delley, B., Veprek, S. & Stampfl, C. (2006*c*). Superhard nitride-based nanocomposites: Role of interfaces and effect of impurities. *Phys Rev Lett* **97**(8), 086102.

Hauert, R. & Patscheider, J. (2000). From alloying to nanocomposites—Improved performance of hard coatings. *Adv Eng Mater* **2**(5), 247–259.

MacKenzie, M., Weatherly, G.C., McComb, D.W. & Craven, A.J. (2005). Electron energy loss spectroscopy of a TiAlN coating on stainless steel. *Scr Mater* **53**(8), 983–987.

Mahieu, S., Ghekiere, P., Depla, D. & De Gryse, R. (2006). Biaxial alignment in sputter deposited thin films. *Thin Solid Films* **515**(4), 1229–1249.

Mayer, M. (1997). *SIMNRA User's Guide*. Garching, Germany: Max-Plank-Institut für Plasmaphysik.

Mayrhofer, P.H., Mitterer, C., Hultman, L. & Clemens, H. (2006). Microstructural design of hard coatings. *Prog Mater Sci* **51**(8), 1032–1114.

Nakonechna, O., Cselle, T., Moretein, M. & Karimi, A. (2004). On the behaviour of indentation fracture in TiAlSiN hard thin films. *Thin Solid Films* **447–448**, 447–448.

PalDey, S. & Deevi, S.C. (2003). Single layer and multilayer wear resistant coatings of (Ti,Al)N: A review. *Mater Sci Eng A-Struct* **342**(1–2), 58–79.

Park, I.-W. & Kim, K.H. (2003). Role of amorphous Si_3N_4 in the microhardness of Ti-Al-Si-N nanocomposite films. *J Korean Phys Soc* **42**(6), 783–786.

Perez-Omil, J.A. (1994). Interpretación sistemática de imágenes de microscopía electrónica de alta resolución de materiales policristalinos. Estudio de catalizadores metálicos soportados. In *Departamento de Ciencia de Materiales e Ingenieria Metalurgica y Quimica Inorganica*. Cadiz, Spain: University of Cadiz.

Philippon, D., Godinho, V., Nagy, P.M., Delplancke-Ogletree, M.P. & Fernandez, A. (2011). Endurance of TiAlSiN coatings: Effect of Si and bias on wear and adhesion. *Wear* **270**(7–8), 541–549.

Ribeiro, E., Malczyk, A., Carvalho, S., Rebouta, L., Fernandes, J.V., Alves, E. & Miranda, A.S. (2002). Effects of ion bombardment on properties of d.c. sputtered superhard (Ti,Si, Al)N nanocomposite coatings. *Surf Coat Technol* **151–152**, 515–520.

Soderberg, H., Oden, M., Larsson, T., Hultman, L. & Molina-Aldareguia, J.M. (2006). Epitaxial stabilization of cubic-SiN_x in TiN/SiN_x multilayers. *Appl Phys Lett* **88**(19), 191902.

Tanaka, Y., Ichimiya, N., Onishi, Y. & Yamada, Y. (2001). Structure and properties of Al-Ti-Si-N coatings prepared by the cathodic arc ion plating method for high speed cutting applications. *Surf Coat Technol* **146–147**, 215–221.

Thornton, J.A. (1977). High rate thick film growth. *Ann Rev Mater Sci* **7**, 239–260.

Vaz, F., Rebouta, L., Almeida, B., Goudeau, P., Pacaud, J., Riviere, J.P. & Sousa, J.B.E. (1999). Structural analysis of

$Ti_{1-x}Si_xNy$ nanocomposite films prepared by reactive magnetron sputtering. *Surf Coat Technol* **120**, 166–172.

Vaz, F., Rebouta, L., Goudeau, P., Pacaud, J., Garem, H., Riviere, J.P., Cavaleiro, A. & Alves, E. (2000). Characterisation of $Ti_{1-x}Si_xNy$ nanocomposite films. *Surf Coat Technol* **133**, 307–313.

Veprek, S. & Jilek, M. (2003). Superhard and functional nanocomposites formed by self-organization in comparison with hardening of coatings by energetic ion bombardment during their deposition. *Rev Adv Mater Sci* **5**, 6–16.

Veprek, S., Karvankova, P. & Veprek-Heijman, M.G. (2005*a*). Possible role of oxygen impurities in degradation of nc-TiN/a-Si3N4 nanocomposites. *J Vac Sci Technol B* **23**(6), 17–21.

Veprek, S. & Reiprich, S. (1995). A concept for the design of novel superhard coatings. *Thin Solid Films* **268**, 64–71.

Veprek, S., Veprek-Heijman, M.G.J., Karvankova, P. & Prochazka, J. (2005*b*). Different approaches to superhard coatings and nanocomposites. *Thin Solid Films* **476**(1), 1–29.

Veprek, S., Zhang, R.F., Veprek-Heijman, M.G.J., Sheng, S.H. & Argon, A.S. (2010). Superhard nanocomposites: Origin of hardness enhancement, properties and applications. *Surf Coat Technol* **204**(12–13), 1898–1906.

Zhang, R.F. & Veprek, S. (2006). On the spinodal nature of the phase segregation and formation of stable nanostructure in the Ti-Si-N system. *Mater Sci Eng A* **424**(1–2), 128–137.